Application of an Angular Momentum Balance Method for Investigating Numerical Accuracy in Swirling Flow

H. Nilsson

L. Davidson

Department of Thermo and Fluid Dynamics,
Chalmers,
SE-412 96 Göteborg, Sweden

This work derives and applies a method for the investigation of numerical accuracy in computational fluid dynamics. The method is used to investigate discretization errors in computations of swirling flow in water turbines. The work focuses on the conservation of a subset of the angular momentum equations that is particularly important to swirling flow in water turbines. The method is based on the fact that the discretized angular momentum equations are not necessarily conserved when the discretized linear momentum equations are solved. However, the method can be used to investigate the effect of discretization on any equation that should be conserved in the correct solution, and the application is not limited to water turbines. Computations made for two Kaplan water turbine runners and a simplified geometry of one of the Kaplan runner ducts are investigated to highlight the general and simple applicability of the method.
[DOI: 10.1115/1.1595673]

1 Background

The use of computational fluid dynamics (CFD) in industry has increased dramatically in recent decades and is now used in many fields as a complement to model testing. Computational results obtained in industrial applications are usually claimed to be qualitatively correct, i.e., they can be used to identify trends but not to establish the quantitatively correct values. There are several reasons why the industrial computational results are not quantitatively correct. First, the physics of the applications and the boundary conditions are approximated using more or less sophisticated methods. Secondly, the resulting approximated physical application is computed by a numerical method that uses further approximations and computational limitations.

To study the accuracy of the numerical method, an assumption can be made that the physics of the application and the boundary conditions are approximated consistently. The accuracy of a computation then depends on the resolution of the discretized problem. A sufficiently fine resolution will thus give the correct solution to the approximated problem if the iterative convergence and round-off errors are small. Fine resolutions cannot be used in industrial applications, however, because of restrictions on computational power and time limitations. The resolutions used in industrial applications are usually not even close to a sufficiently fine resolution. This has lead to an increased interest in methods for studying the accuracy of CFD results, [1,2], and many scientific journals have adopted statement policies about this, [3,4].

When CFD is applied to turbulent flow in complex geometries it is often difficult to obtain an iteratively converged solution, i.e., a solution that satisfies the discretized equations, for the reason that the preferred higher order discretization schemes are highly unstable when the computational grid has very skewed and thin control volumes. One way of dealing with this is to use stable discretization schemes. A number of discretization schemes of varying stability are available in the literature. Depending on the complexity of the flow and the geometry, a discretization scheme that gives an iteratively converged solution usually has an observed discretization order that lies between the first and second order. Figure 1 shows the computed flow above and below a Kaplan runner using the first-order hybrid scheme and the second-order Van Leer scheme. The influence of the discretization scheme is striking.

Stable discretization schemes introduce discretization errors that must be investigated before it is possible to achieve reliable computational results.

One approach to studying the accuracy of CFD results is to look at the sensitivity to grid refinement using the Richardson extrapolation method, [5–7]. The Richardson method uses results from three grids of different refinement to estimate the grid convergence error. If h is a geometric discretization parameter representative of the grid spacing of the finest grid ($h_1=h$), the subsequent grids are coarsened according to $h_2=rh$ and $h_3=r^2h$. The refinement parameter can for instance be chosen to be $r=2$. The main requirement of the Richardson method is that the solutions at all the grids must be in the asymptotic range. This requirement can be met in some cases. In general three-dimensional industrial computations, however, where it is difficult to get even the finest solution in the asymptotic range, the method cannot be used to its full extent, [8,9]. Another major drawback of the method is that time constraints do not allow computations on several grids in industry. The original Richardson paper, [10], examined the difference between a low-order solution and a high-order solution on the same grid. This requires computations of two solutions, which is time-consuming, and makes it necessary to obtain a high-order computation, which is not always the case in industrial CFD. A fast and simple method that investigates the discretization error of a single solution on a single (coarse) grid is therefore needed.

The present method uses a single computational result from a single grid to investigate the accuracy of that computational result. Most CFD codes use conservation of mass and linear momentum to compute the flow. Hence, imbalances in angular momentum, kinetic energy and higher moments reflect the numerical accuracy, [11,12]. The CFD codes may be rewritten to conserve other than mass and linear momentum, but, in any numerical approach, there will be nonconserved quantities that can serve as candidates for numerical accuracy assessment. Since all quantities of the flow cannot be investigated, it is necessary to choose quantities that are

Contributed by the Fluids Engineering Division for publication in the JOURNAL OF FLUIDS ENGINEERING. Manuscript received by the Fluids Engineering Division Nov. 15, 2001; revised manuscript received Feb. 23, 2003. Associate Editors: G. Karniadakis.

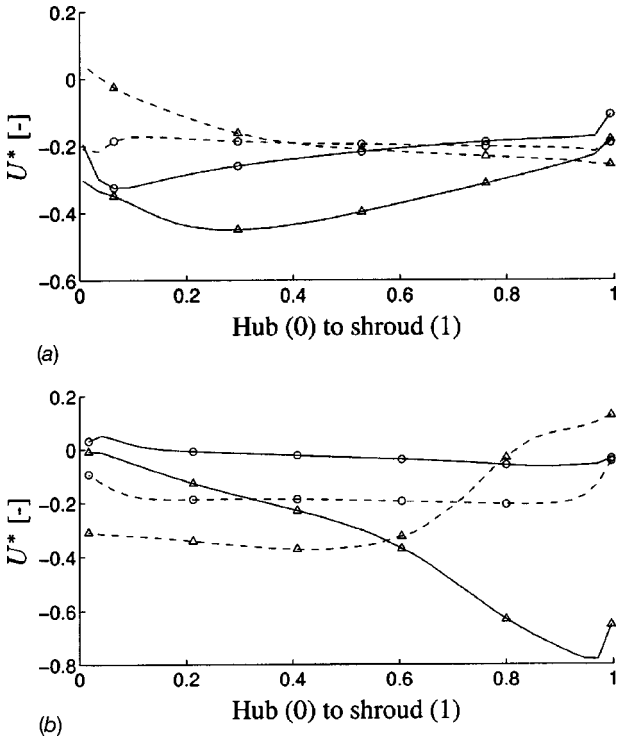

Fig. 1 Circumferentially averaged velocity coefficients above and below a Kaplan runner (Kaplan 1). Solid lines: tangential velocity; dashed lines: axial velocity. Markers: △: first-order hybrid scheme; ○: second-order Van Leer scheme. The velocities are normalized by the runner radius and the runner angular velocity. (*a*) Above the runner, (*b*) below the runner.

particularly important to the flow. A set of important quantities can be specified for each industrial application. The method described in this work can be used to estimate the accuracy with respect to those quantities. When all important quantities of the flow are conserved, the computational results can be considered correct. Angular momentum is one important quantity in swirling flow in water turbines, which is studied in the present work.

2 Derivation of the Angular Momentum Balance

The derivation of the angular momentum balance starts with the Reynolds transport theorem for an arbitrarily moving deformable control volume, [13,14],

$$\frac{dB_{\text{syst}}}{dt} = \frac{d}{dt}\left(\int_{CV} \beta\rho dV \right) + \int_{CS} \beta\rho(\mathbf{U_r}\cdot\mathbf{n})dA$$

where B is a property of the fluid, $\beta = dB/dm$ is the *intensive* value or B per unit mass, and dB_{syst}/dt is the rate of change of B of a system (material region) confined in a control volume that instantaneously comprises the system. This expression is thus a conversion formula between a system and a control volume that instantaneously occupies the same space and, in other words, is a coupling between the Lagrangian and Eulerian descriptions. The velocity relative to that of the control volume surface is $\mathbf{U_r} = \mathbf{U}(\mathbf{r},t) - \mathbf{U}_s(\mathbf{r},t)$, where $\mathbf{U}(\mathbf{r},t)$ is the fluid velocity and $\mathbf{U}_s(\mathbf{r},t)$ is the control volume surface velocity. The Reynolds transport theorem can be used to write all the basic laws in integral form and can thus be used to derive the mass balance ($B=m$, $\beta = dm/dm = 1$), the linear momentum balance (Navier Stokes, $\mathbf{B} = m\mathbf{U}$, $\beta = d m\mathbf{U}/dm = \mathbf{U}$), the energy balance ($B=E$, $\beta = dE/dm = e$), and the angular momentum balance ($\mathbf{B} = \mathbf{H}_o = \int_{\text{syst}} (\mathbf{r}\times\mathbf{U}) dm$, $\beta = d\mathbf{H}_o/dm = \mathbf{r}\times\mathbf{U}$).

The angular momentum balance for an arbitrarily moving deformable control volume is

$$\left.\frac{d\mathbf{H}_o}{dt}\right|_{\text{syst}} = \frac{d}{dt}\left(\int_{CV} (\mathbf{r}\times\mathbf{U})\rho dV \right) + \int_{CS} (\mathbf{r}\times\mathbf{U})\rho(\mathbf{U_r}\cdot\mathbf{n})dA. \quad (1)$$

According to the laws of mechanics, the rate of change of the angular momentum of the system is equal to the sum of all the moments about an arbitrary point o acting on a control volume that instantaneously comprises the system, yielding an expression for the left-hand side of Eq. (1) as ([15])

$$\left.\frac{d\mathbf{H}_o}{dt}\right|_{\text{syst}} = \int_{CS} \mathbf{r}\times\mathbf{F}_s dA + \int_{CV} \mathbf{r}\times\mathbf{F}_b \rho dV - \int_{CV} (\mathbf{r}\times\mathbf{a})\rho dV, \quad (2)$$

where $\mathbf{F}_s$ is the surface force (both viscous, turbulent shear, and normal forces) per unit area acting on the control volume surface and $\mathbf{F}_b$ is the body force per unit mass acting inside the control volume. The vector, $\mathbf{a}$, is the acceleration of the coordinate system, [14],

$$\mathbf{a} = \frac{d^2\mathbf{R}}{dt^2} + \frac{d\boldsymbol{\Omega}}{dt}\times\mathbf{r} + 2\boldsymbol{\Omega}\times\mathbf{U} + \boldsymbol{\Omega}\times(\boldsymbol{\Omega}\times\mathbf{r}), \quad (3)$$

where $\mathbf{R}$ is the position vector of the origin of the noninertial coordinate system relative to an inertial coordinate system, $\mathbf{r}$ is the position vector relative to the non-inertial coordinate system, and $\boldsymbol{\Omega}$ is the angular velocity of the noninertial coordinate system. The terms on the right hand side in the equation correspond to system acceleration, system angular acceleration, Coriolis acceleration and centripetal acceleration.

If the control volume is nondeformable and the flow is steady, the time derivative of the volume integral in Eq. (1) vanishes. Further, if the control volume is rotating at a constant $\boldsymbol{\Omega}$ about a stationary origin, the angular momentum balance (Eqs. (1)–(3)) reads

$$\int_{CS} \mathbf{r}\times\mathbf{F}_s dA + \int_{CV} \mathbf{r}\times\mathbf{F}_b \rho dV - \int_{CV} \mathbf{r}\times(2\boldsymbol{\Omega}\times\mathbf{U})\rho dV - \int_{CV} \mathbf{r}\times(\boldsymbol{\Omega}\times(\boldsymbol{\Omega}\times\mathbf{r}))\rho dV = \int_{CS} (\mathbf{r}\times\mathbf{U})\rho(\mathbf{U}\cdot\mathbf{n})dA. \quad (4)$$

This is an extremely complicated relation that contains all the features of the linear momentum balance. In addition, it should be recalled that it was derived from the change in angular momentum about point o, which has not yet been specified. Relation (4) is obviously valid for all possible choices of o!

If the position vector, $\mathbf{r}$, can be approximated as constant over the volume of integration, the angular momentum and linear momentum balances are equivalent in continuum mechanics, [13], and the angular momentum balance can be derived from the vector product of $\mathbf{r}$ and the linear momentum balance. However, since the computational control volumes are not infinitesimal, the discretized angular momentum balance is not necessarily satisfied simply because the discretized linear momentum balance is satisfied. It is thus up to the discretization scheme to conserve both angular and linear momentum.

2.1 Angular Momentum Balance in Turbomachinery. In turbomachinery, the axial component of the angular momentum balance about the axis of rotation transfers torque to the rotating shaft. Assuming that $\boldsymbol{\Omega} = \Omega\mathbf{e}_z$ ($\mathbf{e}_z$ is the unit vector in the z-direction) is aligned with the shaft, the axial component of the angular momentum balance (Eq. (4)) about the axis of rotation reads

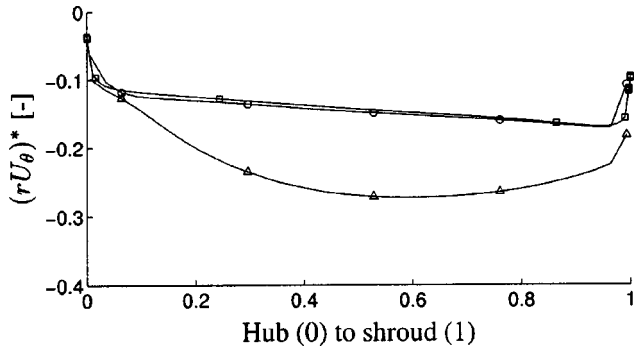

Fig. 2 Angular momentum distributions at the inlet and a section before the runner of a Kaplan runner (Kaplan 1). The distribution at the inlet should be approximately conserved at the section before the runner in a correct solution, i.e., the curves should coincide. Markers: □: inlet distribution; △: first-order hybrid scheme, before the runner; ○: second-order Van Leer scheme, before the runner. The angular momentum is normalized by the runner radius and the runner angular velocity.

$$\int_{CS} rF_{s\theta}dA + \int_{CV} rF_{b\theta}dV + \int_{CV} 2r\Omega U_r \rho dV = \int_{CS} rU_\theta \rho(\mathbf{U}\cdot\mathbf{n})dA \tag{5}$$

where r is the cylindrical radial direction and θ is the tangential direction. The term involving Ω originates from the Coriolis term of the angular momentum balance. There is no effect of the centripetal term, however, since the coordinate system rotation vector, $\mathbf{\Omega}$, is aligned with the axial component of the balance. Further, if gravity, as in the present work, is the only body force, $\int_{CV} rF_{b\theta}dV = 0$. Equation (5) is the central equation in the present work.

Equation (5) can be further reduced for simple investigations of the flow in turbomachines. This is done in the remainder of this section. When applied to a thin stationary axisymmetric stream tube ($r \approx$ const at inlet and outlet) with uniform inlet (index 1) and outlet (index 2) velocities and negligible surface forces, Eq. (5) is reduced to

$$\int_{CV} rF_{b\theta}dV = \Delta\dot{m}(r_2U_{\theta 2} - r_1U_{\theta 1})$$

where $\Delta\dot{m}$ is the mass flow through the stream tube. If $F_{b\theta}$ includes all the tangential body forces from the blades in a turbomachine, we obtain the power balance for the stream tube, [15],

$$-\Delta P_{\text{shaft}} = \Delta\dot{m}\Omega(r_2U_{\theta 2} - r_1U_{\theta 1}). \tag{6}$$

This is the *general Euler equation for turbomachinery*, [15], relating the input shaft power to the change in angular momentum for a thin axisymmetric stream tube, which highlights the importance of the angular momentum balance in this kind of flow.

Equation (6) can be used to verify the numerical results to some extent. One can assume that the thicknesses of the stream tubes through the domain are proportional to the channel width, and that the mass flow through all the stream tubes is the same, [16]. These are not accurate assumptions, which is one of the reasons that this simplified method is not complete. Further, the shaft power in each stream tube is difficult to obtain, and thus the general Euler equation is not easily applicable in the region where the runner blades are located. However, the distribution of rU_θ should be approximately conserved in each stream tube in regions where there are no runner blades ($\Delta P_{\text{shaft}} = 0$). Figure 2 shows the angular momentum distribution of the circumferentially averaged flow at the inlet and a section above the runner of a Kaplan runner (the Kaplan 1 runner described later) for both the first-order hybrid and the second-order Van Leer discretization schemes (using the tangential velocities in Fig. 1(*a*)). It is obvious that the hybrid computation does not satisfy the general Euler equation while the Van Leer computation works well. The Van Leer computations were carried out and analyzed by Nilsson and Davidson [17] (the k15 case), which gives detailed information on the analysis in Fig. 2.

The present work uses Eq. (5), without further assumptions, to investigate numerical accuracy of the computational results.

3 The Computational Method

The computations used for the investigations in the present work were made using the CALC-PMB finite volume CFD code. The main features of the CALC-PMB CFD code are its use of conformal block structured boundary fitted coordinates, a pressure correction scheme (SIMPLEC [18]), Cartesian velocity components as the principal unknowns, and a collocated grid arrangement together with Rhie and Chow interpolation. The computational blocks are solved in parallel with Dirichlet-Dirichlet coupling using PVM (parallel virtual machine) or MPI (message passing interface). The parallel efficiency is excellent, with super scalar speed-up for load balanced applications, [19]. The ICEM CFD/CAE grid generator is used for grid generation, and Ensight and Matlab are used for post-processing.

Coriolis and centripetal effects are included in the momentum equations when the computational domain is rotating, but the low-Reynolds $k-\omega$ turbulence model of Wilcox [20], which can be integrated all the way to the wall, is used without terms for rotational effects. This is common in turbomachinery computations for reasons of numerical stability and the small impact of such terms in these kinds of industrial applications.

This work investigates the computational results obtained using two different discretization schemes, the hybrid scheme, and the Van Leer scheme. Equations and discretization schemes are described in the following sections.

3.1 Equations. The steady Reynolds time-averaged continuity and Navier-Stokes equations for incompressible flow in a rotating frame of reference read ([21,22])

$$\frac{\partial \rho U_i}{\partial x_i} = 0$$

$$\frac{\partial \rho U_i U_j}{\partial x_j} = -\frac{\partial P}{\partial x_i} + \frac{\partial}{\partial x_j}\left((\mu + \mu_t)\frac{\partial U_i}{\partial x_j}\right) + \rho g_i - \rho\epsilon_{ijk}\epsilon_{klm}\Omega_j\Omega_l x_m - 2\rho\epsilon_{ijk}\Omega_j U_k$$

where $-\epsilon_{ijk}\epsilon_{klm}\Omega_j\Omega_l x_m$ is the centripetal term and $-2\epsilon_{ijk}\Omega_j U_k$ is the Coriolis term, owing to the rotating coordinate system. Because of the potential nature of the pressure, gravitational and centripetal terms, [22], they are put together during the computations in what is often referred to as a *reduced* pressure gradient

$$-\frac{\partial P^*}{\partial x_i} = -\frac{\partial P}{\partial x_i} + \rho g_i - \rho\epsilon_{ijk}\epsilon_{klm}\Omega_j\Omega_l x_m .$$

Thus, a relation for the *reduced* pressure is

$$P^* = P - \rho g_i x_i + \rho\epsilon_{ijk}\epsilon_{klm}\Omega_j\Omega_l x_m x_i .$$

In post-processing, the variation of the gravity term is assumed to be negligible and the centripetal term is simply subtracted from the *reduced* pressure.

The $k-\omega$ model of Wilcox [20] for the turbulent kinetic energy, k, and the specific dissipation rate, ω, reads

$$\frac{\partial \rho U_j k}{\partial x_j} = \frac{\partial}{\partial x_j}\left[\left(\mu + \frac{\mu_t}{\sigma_k}\right)\frac{\partial k}{\partial x_j}\right] + P_k - \rho\beta^* \omega k$$

$$\frac{\partial \rho U_j \omega}{\partial x_j} = \frac{\partial}{\partial x_j}\left[\left(\mu + \frac{\mu_t}{\sigma_\omega}\right)\frac{\partial \omega}{\partial x_j}\right] + \frac{\omega}{k}(c_{\omega 1} P_k - c_{\omega 2}\rho k \omega)$$

where the turbulent viscosity, μ_t, is defined as

$$\mu_t = \rho \frac{k}{\omega}.$$

The production term reads

$$P_k = \mu_t\left(\frac{\partial U_i}{\partial x_j} + \frac{\partial U_j}{\partial x_i}\right)\frac{\partial U_i}{\partial x_j}$$

and the closure coefficients are given by

$$\beta^* = 0.09, \quad c_{\omega 1} = \frac{5}{9}, \quad c_{\omega 2} = \frac{3}{40}, \quad \sigma_k = 2 \quad \text{and} \quad \sigma_\omega = 2.$$

A no-slip wall boundary condition is applied for the velocities and $k = 0$ at the walls. The specific dissipation at the first node normal to the wall (at $y^+ < 2.5$) is set to $\omega = 6\nu/(C_{\omega 2} n^2)$, where n denotes the normal distance to the wall. For the pressure, $\partial^2 P/\partial n^2 = 0$ at all boundaries. Dirichlet boundary conditions are applied at the inlet and Neumann boundary conditions are applied at the outlet for the velocity components and for the turbulent quantities.

3.2 Discretization Schemes. To solve the discretized linear momentum equations, the fluxes through the faces of the computational control volumes must be known. Since all variables are calculated at the nodes, some kind of interpolation must be used to obtain the fluxes through the computational control volume faces. A number of ways of doing this are described in the literature. This work studies the numerical solutions obtained when using the hybrid and the Van Leer [23] discretization schemes. Both discretization schemes are bounded and use upwinding for the convective terms. They are briefly described in the following sections.

3.2.1 The Hybrid Scheme. The hybrid scheme is a combination of the central and the first-order upwind schemes. It uses central differencing if the magnitude of the Peclet number is below two and first-order upwind differencing otherwise, i.e.,

$$\Phi_e = \Phi_P \quad \text{for } U_e > 0 \quad \text{and} \quad |\mathrm{Pe}_e| \geq 2$$

$$\Phi_e = \Phi_E \quad \text{for } U_e < 0 \quad \text{and} \quad |\mathrm{Pe}_e| \geq 2$$

$$\Phi_e = f_e \Phi_E + (1 - f_e)\Phi_P \quad \text{for } |\mathrm{Pe}_e| < 2.$$

The Peclet number reads

$$\mathrm{Pe}_e = \frac{F_e}{D_e}$$

where F_e is the convective mass flux and D_e is the diffusion flux at the computational control volume faces. The factor f_e that appears in the central scheme is a linear interpolation factor that allows the grid to be nonuniform; for uniform grids, $f_e = 0.5$. The hybrid scheme thus uses the first-order upwind scheme if convection is dominant and the central scheme if diffusion is not negligible. The diffusion is discretized using central differencing for $|\mathrm{Pe}_e| < 2$ and is neglected otherwise.

The major drawback of the hybrid scheme is that convection is dominant in most flows, and the scheme can thus be regarded as a first-order upwind scheme.

3.2.2 The Van Leer Scheme. The scheme of Van Leer [23] is of second-order accuracy except at local minima or maxima, where its accuracy is of the first order. One advantage of this scheme is that it is bounded. For the east face, it can be written

$$U_e > 0 \Rightarrow \begin{cases} \Phi_e = \Phi_P & \text{if } |\Phi_E - 2\Phi_P + \Phi_W| \geq |\Phi_E - \Phi_W| \\ \Phi_e = \Phi_P + \dfrac{(\Phi_E - \Phi_P)(\Phi_P - \Phi_W)}{\Phi_E - \Phi_W} & \text{otherwise} \end{cases}$$

$$U_e < 0 \Rightarrow \begin{cases} \Phi_e = \Phi_E & \text{if } |\Phi_P - 2\Phi_E + \Phi_{EE}| \geq |\Phi_P - \Phi_{EE}| \\ \Phi_e = \Phi_E + \dfrac{(\Phi_P - \Phi_E)(\Phi_E - \Phi_{EE})}{\Phi_P - \Phi_{EE}} & \text{otherwise} \end{cases}.$$

The diffusion is discretized using central differencing.

This scheme is thus a bounded first-order upwind scheme with a correction term, which makes it second-order accurate.

3.3 Convergence, Verification, and Validation. An iteratively converged solution is assumed to have been reached when the largest normalized residual of the momentum equations, the continuity equation and the turbulence equations is reduced to 10^{-3}, [24]. The residuals of the momentum equation are normalized by the sum of the mass flow through the turbine and the mass flow through the periodic surfaces multiplied by the largest velocity component in the computational domain. The residual of the continuity equation is normalized by the sum of the mass flow through the turbine and the mass flow through the periodic surfaces. The residuals of the turbulence equations are normalized by the largest residual during the iterations.

The iteratively converged results of a correctly implemented finite volume method should be conservative with respect to the computed equations. The computational results of the continuity and linear momentum equations have been verified by the method described in this work. The result from this verification corresponds to the iterative convergence limit. The information obtained from the angular momentum balance can not be obtained from the mass or linear momentum balances, however, since the finite volume formulation conserves mass and linear momentum when the residuals are small.

The CALC-PMB CFD code has been extensively validated against the GAMM Francis runner, the Hölleforsen (Turbine 99–II) Kaplan runner, the Hölleforsen distributor and academic test cases, [25]. The code has also been used and validated in other industrial applications, such as: LES of the flow around a simplified bus, LES of a high-lift air foil and heat transfer in gas turbines.

The code uses double precision real numbers to avoid numerical cancellation.

4 Cases

The angular momentum balance method described in the present work is applied to the flow in water turbines. There are numerous types and configurations of water turbines, each optimized for the conditions of the specific power plant. The water turbines studied in this work are low-head Kaplan turbines, which are the most common water turbines in Sweden.

The geometry and flow features in the vicinity of a Kaplan water turbine runner comprises an axisymmetric duct with radial swirling inflow above the runner and axial (ideally nonswirling) flow through a short axisymmetric diffusor below the runner. The angular momentum balance method is applied to two Kaplan runners and a simplified geometry of the axisymmetric duct of one of the Kaplan runners without the runner blades (see Fig. 3).

The cases are briefly described in the following sections.

4.1 Simplified Geometry. Figure 4 shows the meridional contour of the simplified geometry and two computational grids with 14,378 and 31,521 control volumes. The complete geometry is the axisymmetric volume obtained from revolving this geometry around the *Z*-axis. The grids have different grid density in the through-flow direction and similar grid distributions in the other two directions. There are seven computational control volumes in the periodic direction, covering 10 deg of the total circumference. Periodic boundary conditions are used in the circumferential di-

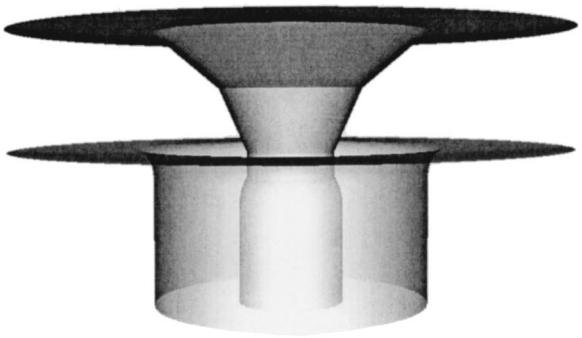

(*a*)

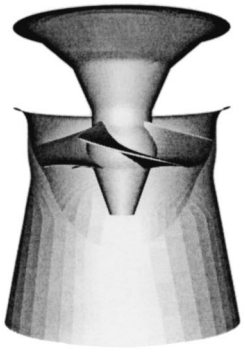

(*b*)

(*c*)

Fig. 3 The three geometries studied in this work. In all cases the flow is swirling radially inwards at the top and axially downwards at the bottom. (*a*) The simplified geometry, (*b*) Kaplan 1, (*c*) Kaplan 2.

rection. The velocity profile at the inlet is a turbulent 1/7 profile with a swirling component, [24], and the steady axisymmetric flow in the inertial coordinate system is computed.

4.2 Kaplan Runners. Two different Kaplan runners are investigated in the present work. For both cases, the steady flow is computed in a single rotating blade passage employing periodic boundary conditions. Inlet boundary conditions are taken from separate computations of the flow in the upstream guide vane passage.

Detailed information on the first Kaplan runner case (denoted Kaplan 1) can be found in the literature, [24,25], where it is denoted case k15. The simplified geometry in this work is the same as the upper part of the duct of this Kaplan runner, where the error is greatest for the hybrid discretization scheme.

The computational results of the flow in the Hölleforsen Kaplan runner (denoted Kaplan 2) were thoroughly investigated and validated against measurements at the Turbine 99–II workshop. The investigations included in the present work use the computation that was denoted the standard case in the workshop paper, [26], which used the Van Leer discretization scheme. A computation with the hybrid discretization scheme has also been made to show the difference in the angular momentum balance between the two schemes.

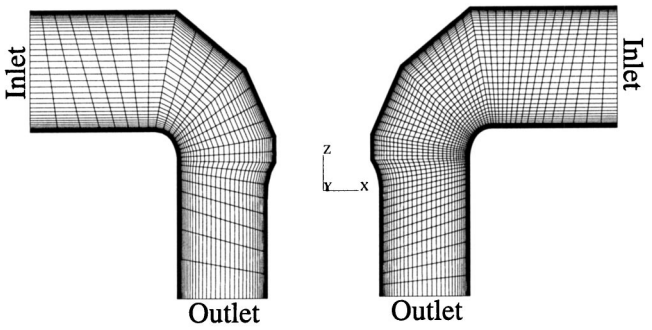

Fig. 4 Meridional view of the coarse (left) and fine (right) grid of the simplified geometry. The grid densities and distributions differ mainly in the through-flow direction.

Both Kaplan cases include the clearance between the runner blade tips and the shroud, which makes structured multiblock grid generation very complicated.

5 The Angular Momentum Balance Method

5.1 Implementation. The fundamental idea of the angular momentum balance method is to compute the flux of angular momentum through the computational control volume faces using exactly the same discretization scheme as was used for the flux of linear momentum in the CFD solver (see Section 3.2). It is very important that this implementation is made correctly since small errors in computing the fluxes make it impossible to investigate the balance error. The angular momentum fluxes are used to compute a control volume angular momentum balance error by summing up the flux into the control volume and generation inside the control volume, and normalizing by the flux into the computational domain, i.e., (c.f. Eq. (5))

$$\epsilon = \left(\int_{CS} rF_{s\theta} dA + \int_{CV} rF_{b\theta} dV + \int_{CV} 2r\Omega U_r \rho dV - \int_{CS} rU_\theta \rho (\mathbf{U}\cdot\mathbf{n}) dA \right) \Big/ \int_{\text{INLET}} rU_\theta \rho (\mathbf{U}\cdot\mathbf{n}) dA .$$

The control volume investigated can be a computational control volume or a control volume that comprises several of the computational control volumes. When computing a balance error over several computational control volumes, a summation of the balance errors over the computational control volumes cancels the fluxes through internal faces, which results in a balance error of the composite control volume.

In the present work the angular momentum balance method is applied to through-flow investigations, [27]. Applying the method between two cross-flow planes (axisymmetric in turbomachine runners) yields the angular momentum balance error between those planes. Placing the first cross-flow plane at the inlet and moving the second cross-flow plane from the inlet to the outlet (from plane 1 to plane 26 in Fig. 5(*a*)) yields the global angular momentum balance error evolution along the flow path. This can be easily done in the CFD code if there are cross-flow grid planes that can serve as boundaries for the control volumes investigated.

A more general method for summing the balance error over a subdomain of the computational domain is to save the computational control volume balances as an element-based (constant in

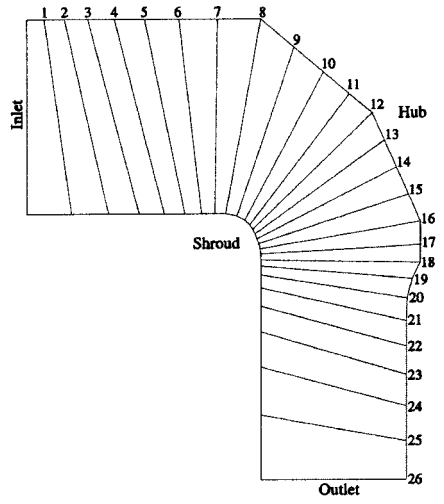

(*a*)

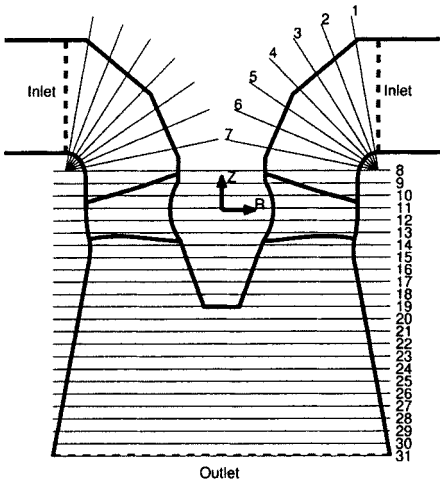

(*b*)

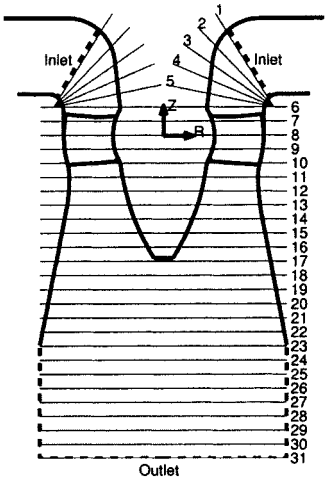

(*c*)

Fig. 5 Definitions of the cross-flow axisymmetric surfaces. The numbered surfaces (represented by thin lines) are grid surfaces for the simplified case and general control surfaces for the Kaplan cases. (*a*) The simplified geometry with numbered axisymmetric cross-flow grid surfaces corresponding to the coarse grid. (*b*) The meridional contour of the Kaplan 1 runner (thick lines). The dashed lines show the computational domain. (*c*) The meridional contour of the Kaplan 2 runner (thick lines). The dashed lines show the computational domain.

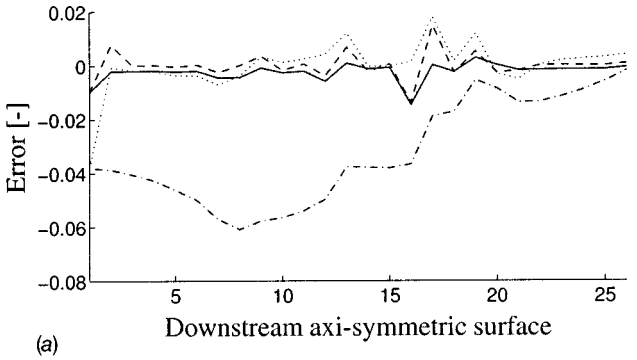

(*a*)

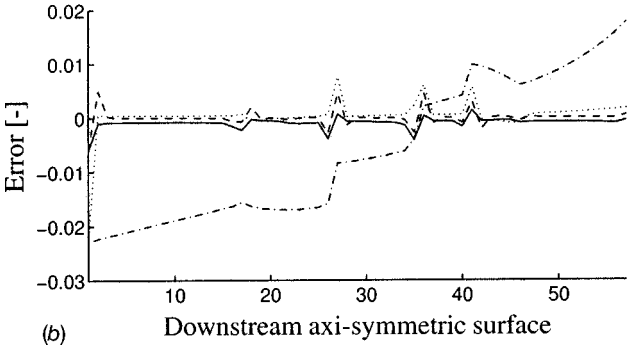

(*b*)

Fig. 6 Local and cumulative error distributions from inlet to outlet of the simplified geometry. Dashed line: Van-Leer, local error; dotted line: hybrid, local error; solid line: Van-Leer, cumulative error; dashed-dotted line: hybrid, cumulative error. (*a*) Coarse grid, (*b*) fine grid.

each computational control volume) error density, i.e., the balance divided by the volume of the computational control volume. Using a post-processing tool such as Ensight, the sum over any subdomain can be derived by an element-based volume integral of the error density over the subdomain. There is then no need for explicit grid planes at the cross-flow surfaces, and they can cut arbitrarily through the geometry (see Figs. 5(*b,c*)). The only requirements on the post-processing tool are that it can cut out arbitrary parts of the computational domain and compute the volumes of the computational control volumes correctly. The element-based volume integral is then obtained by multiplying the volume of the computational control volume by the local balance, which is constant in each computational control volume. The overall balance and volume of the computational domain were conserved in the analysis by Ensight, and the investigation of the simplified geometry gave the same result in both the analysis by the CFD code and in the analysis by Ensight. This shows that no significant errors are introduced in the post-processing by Ensight.

5.2 Results. Figure 6 shows the local (between two neighboring axisymmetric surfaces) and cumulative (from the inlet) angular momentum balance error distributions from inlet to outlet (see Section 5.1) in the simplified geometry. The overall balance (from inlet to outlet) is obviously not necessarily representative of the accuracy of the computations since the errors in different parts of the domain might cancel each other. The coarse grid hybrid analysis in Fig. 6(*a*) highlights this problem, where the total error of the domain is small but the error in different subdomains is large.

Both the hybrid and the Van Leer discretization schemes yield small local errors. The cumulative errors show, however, that the hybrid scheme accumulates the local errors while the Van Leer scheme cancels the local errors. Both schemes have problems at

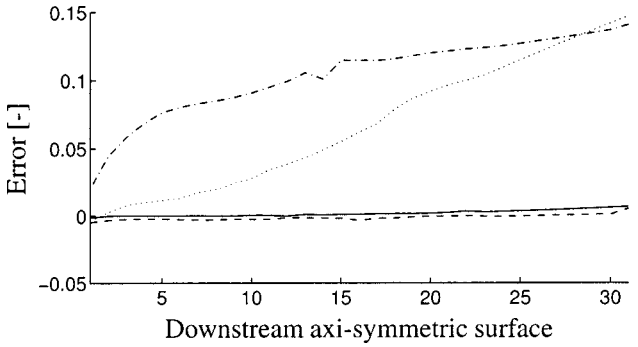

Fig. 7 Cumulative error distributions from inlet to outlet of the Kaplan cases. Dashed line: Van-Leer, Kaplan 1; dashed-dotted line: hybrid, Kaplan 1; solid line: Van-Leer, Kaplan 2; dotted line: hybrid, Kaplan 2.

the inlet and at sharp geometric corners (located at computational control volume planes 8, 12, 16, and 18 for the coarse grid and 17, 26, 35, and 40 for the fine grid).

Figure 7 shows the cumulative angular momentum balance error distributions in the Kaplan runners from inlet to outlet (see Section 5.1). The angular momentum balance method clearly shows the difference between the Van Leer scheme and the hybrid scheme. The hybrid scheme accumulates the local errors while the Van Leer scheme cancels the local errors.

The analysis shows that the hybrid scheme performs worst in the first part of the Kaplan 1 computational domain and best in the first part of the Kaplan 2 computational domain (from the inlet to axisymmetric surface 5).

Table 1 shows the global estimations of the angular momentum balance error, which correspond to the overall cumulative values in Figs. 6 and 7. The global angular momentum balance error of the hybrid scheme are about 30 times larger than that of the Van Leer scheme in the Kaplan cases.

It may seem that a 0.7% angular momentum balance error (Table 1, Van Leer, Kaplan 2) is rather good, but there are at least two reasons why the error should be reduced: (1) the linear momentum is better predicted, (2) water turbine efficiencies are very high (about 95%) and the improvements that can be made are in the range of 0.1% in efficiency. Since the efficiency of water turbines is closely related to the angular momentum balance (see Section 2.1) it is interesting to further investigate the angular momentum balance for the Van Leer scheme. Figure 8 shows iso-surfaces of the largest angular momentum balance error magnitude for the Kaplan 2 Van Leer computations. This gives an indication of where to start the quest for improved results with the Van Leer scheme and the present grid.

6 Conclusion

This work presents a method of investigating the discretization error in swirling flow computations. The method is based on the fact that the discretized angular momentum equations are not necessarily conserved when the discretized linear momentum equations are solved. The method is applied to the first-order hybrid and the second-order Van Leer discretization schemes in swirling flow in water turbines. The angular momentum balance method is applied to through-flow investigations. It is shown that the hybrid scheme cannot be used and that the Van Leer scheme needs improvement to give quantitatively correct results for these kinds of applications. The global angular momentum balance errors of the hybrid scheme are shown to be about 30 times larger than for the Van Leer scheme.

This work has studied only a small part of the angular momentum balance that is important to a single vortex with known features. There are, however, several vortices of unknown features in turbomachinery flow (and most other flows as well) that must also be resolved. A discretization scheme that simultaneously preserves both the linear momentum balance and the *general* angular momentum balance is needed.

Table 1 Global angular momentum balance error estimations

Simplified Case	Van Leer		Hybrid	
	Coarse	Fine	Coarse	Fine
Overall balance	$-6.93\cdot10^{-4}$	$-4.79\cdot10^{-4}$	$-1.92\cdot10^{-3}$	$1.77\cdot10^{-2}$
Kaplan Cases	Van Leer		Hybrid	
	Kaplan 1	Kaplan 2	Kaplan 1	Kaplan 2
Overall balance	$5.41\cdot10^{-3}$	$6.86\cdot10^{-3}$	$1.41\cdot10^{-1}$	$1.47\cdot10^{-1}$

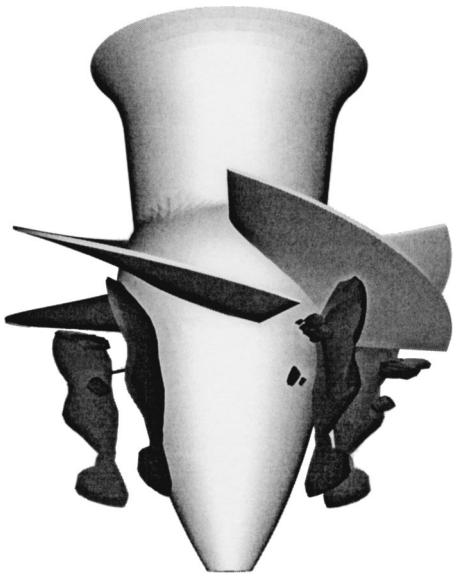

Fig. 8 Iso-surfaces of the absolute value of the computational control volume angular momentum balance indicating where the largest errors are located. The Kaplan 2 case with the Van Leer scheme.

Acknowledgments

This work is financed and supported by ELFORSK (Swedish Electrical Utilities Research and Development Company), the Swedish National Energy Administration and GE Energy (Sweden) AB.

GE Energy (Sweden) AB and its staff, particularly Bengt Nauclér, are gratefully acknowledged for information on geometry and support.

Professor F. Avellan and the staff at IMHEF-EPFL in Lausanne are gratefully acknowledged for their influence during the preliminary stages of this work.

The computational resources used at UNICC, Chalmers, are gratefully acknowledged.

References

[1] Karniadakis, G. E., 2002, "Quantifying Uncertainty in CFD," ASME J. Fluids Eng., **124**, pp. 2–3.
[2] Mehta, U. B., 1998, "Credible Computational Fluid Dynamics Simulations," AIAA J., **36**(5).
[3] AIAA, 1994, "Editorial Policy Statement on Numerical Accuracy and Experimental Uncertainty," AIAA J., **32**.
[4] Journal of Fluids Engineering, 1993, "Editorial Policy Statement on the Control of Numerical Accuracy," ASME J. Fluids Eng., **115**.
[5] Cadafalch, J., Pérez-Segarra, C. D., Còsul, R., and Olivia, A., 2002, "Verifi-

cation of Finite Volume Computations on Steady-State Fluid Flow and Heat Transfer,'' ASME J. Fluids Eng., **124**, pp. 11–21.
[6] Celik, I., and Zhang, W. M., 1995, ''Calculation of Numerical Uncertainty Using Richardson Extrapolation: Application to Some Simple Turbulent Flow Calculations,'' ASME J. Fluids Eng., **117**, pp. 439–445.
[7] Roache, P. J., 1998, ''Verification of Codes and Calculations,'' AIAA J., **36**(5).
[8] Bergström, J., 2000, ''Approximations of Numerical Errors and Boundary Conditions in a Draft Tube,'' *Proceedings from Turbine 99-Workshop on Draft Tube Flow*.
[9] Bergström, J., and Gebart, R., 1999, ''Estimation of Numerical Accuracy for the Flow Field in a Draft Tube,'' Int. J. Numer. Methods Heat Fluid Flow, **9**(4), pp. 472–486.
[10] Richardson, L. F., 1908, ''The Approximate Arithmetical Solution by Finite Differences of Physical Problems Involving Differential Equations, With an Application to the Stresses in a Masonry Dam,'' Transactions of the Royal Society of London, **210**, pp. 307–357.
[11] Chang, S., and Haworth, D. C., 1997, ''Adaptive Grid Refinement Using Cell-Level and Global Imbalances,'' Int. J. Numer. Methods Heat Fluid Flow, **24**, pp. 375–392.
[12] Haworth, D. C., El Tahry, S. H., and Huebler, M. S., 1993, ''A Global Approach to Error Estimation and Physical Diagnostics in Multidimensional Computational Fluid Dynamics,'' Int. J. Numer. Methods Heat Fluid Flow, **17**(1), pp. 75–97.
[13] Panton, R. L., 1996, *Incompressible Flow*, John Wiley and Sons, New York.
[14] White, F. M., 1994, *Fluid Mechanics*, 3rd Ed., McGraw-Hill, New York.
[15] Lakshminarayana, B., 1996, *Fluid Dynamics and Heat Transfer of Turbomachinery*, John Wiley and Sons, New York.
[16] Krivchenko, G., 1994, *Hydraulic Machines: Turbines and Pumps*, 2nd Ed., CRC Press, Boca Raton, FL.
[17] Nilsson, H., and Davidson, L., 2000, ''A Numerical Comparison of Four Operating Conditions in a Kaplan Water Turbine, Focusing on Tip Clearance Flow,'' *Proceedings of the 20th IAHR Symposium, Hydraulic Machinery and Cavitation*.
[18] Van Doormaal, J. P., and Raithby, G. D., 1984, ''Enhancements of the SIMPLE Method for Predicting Incompressible Fluid Flows,'' Numer. Heat Transfer, **7**, pp. 147–163.
[19] Nilsson, H., Dahlström, S., and Davidson, L., 2001, ''Parallel Multiblock CFD Computations Applied to Industrial Cases,'' *Parallel Computational Fluid Dynamics—Trends and Applications*, C. B. Jenssen et al., ed., Elsevier, Amsterdam, pp. 525–532.
[20] Wilcox, D. C., 1988, ''Reassessment of the Scale-Determining Equation for Advanced Turbulence Models,'' AIAA J., **26**(11), pp. 1299–1310.
[21] Davidson, L., 1997, ''An Introduction to Turbulence Models,'' Internal Report, Thermo and Fluid Dynamics, Chalmers University of Technology, Gothenburg Feb.
[22] Kundu, P. K., 1990, *Fluid Mechanics*, Academic Press, San Diego, CA.
[23] van Leer, B., 1974, ''Towards the Ultimate Conservative Difference Scheme. Monotonicity and Conservation Combined in a Second Order Scheme,'' J. Comput. Phys., **14**, pp. 361–370.
[24] Nilsson, H., 1999, ''A Numerical Investigation of the Turbulent Flow in a Kaplan Water Turbine Runner,'' thesis for the degree of Licentiate of Engineering, May, Department of Thermo and Fluid Dynamics, Chalmers University of Technology, Gothenburg.
[25] Nilsson, H., 2002, ''Numerical Investigations of Turbulent Flow in Water Turbines,'' thesis for the degree of Doctor of Philosophy, Department of Thermo and Fluid Dynamics, Chalmers University of Technology, Gothenburg.
[26] Nilsson, H., and Davidson, L., 2001, ''A Numerical Investigation of the Flow in the Wicket Gate and Runner of the Hölleforsen (Turbine 99) Kaplan Turbine Model,'' *Proceedings from Turbine 99 II*.
[27] Santal, O., and Avellan, F., 1992, ''Hydraulic Analysis of Flow Computation Results,'' *Proceedings of the 16th IAHR Symposium*, **2**, pp. 545–554.